Eur. Phys. J. A **6**, 29–36 (1999)

THE EUROPEAN PHYSICAL JOURNAL A

Magnetic moment measurements in the semi-magic nuclei ^{94}Ru and ^{95}Rh after recoil implantation into iron and nickel

A. Jungclaus[1], D. Kast[1], K.P. Lieb[1], C. Lingk[1], C. Teich[1], O. Iordanov[1], T. Härtlein[2], D. Schwalm[2], I.P. Johnstone[3], R. Schwengner[4]

[1] II. Physikalisches Institut, Universität Göttingen, Bunsenstrasse 7-9, D-37073 Göttingen
[2] Max-Planck-Institut für Kernphysik, D-69029 Heidelberg, Germany
[3] Department of Physics, Queen's University, Kingston, Ontario, K7L 3N6 Canada
[4] Institut für Hadronenphysik, FZ Rossendorf, D-01314 Dresden, Germany

Received: 2 June 1999
Communicated by B. Povh

Abstract. The magnetic moments of the 12^+ and 11^- yrast states in ^{94}Ru and of the $25/2^-$, $29/2^+$, and $35/2^+$ levels in ^{95}Rh have been measured via the IMPAD technique. The nuclei were produced in the reaction ^{58}Ni + ^{40}Ca and recoil-implanted into polarized Ni and Fe hosts. The g-factors were deduced from the measured time-integral Larmor precessions. The comparison between the experimental results and large-scale shell model calculations suggests that the 12^+ and 11^- states in ^{94}Ru and the $25/2^-$ level in ^{95}Rh are pure proton states whereas the $29/2^+$ and $35/2^+$ states in ^{95}Rh contain a neutron excitation across the N=50 shell gap. This interpretation supports the conclusion drawn from recent lifetime measurements.

PACS. 21.10.Ky Electromagnetic moments – 21.60.Cs Shell models – 21.60.+j $90 \leq A \leq 149$

1 Introduction

The known excited states in the N = 50 isotones ^{94}Ru and ^{95}Rh [1] can be classified according to their dominant shell model configurations. All the states up to the maximum spin values of 12^+ (4.7 MeV), 13^- (5.6 MeV) and $25/2^+$ (3.7 MeV), $25/2^-$ (3.9 MeV) in ^{94}Ru and ^{95}Rh , respectively, are built from the four resp. five valence protons within the ($p_{1/2}$, $g_{9/2}$) space taking ^{88}Sr as an inert core. To generate higher spins two possibilities exist: protons can be excited from the completely filled $f_{5/2}$, $p_{3/2}$ into the $g_{9/2}$ orbit, or the N = 50 neutron core can be broken by the excitation of a $g_{9/2}$ neutron into the $d_{5/2}$ orbit above the shell gap. At intermediate spins, both processes compete, and the structure of individual states cannot be determined on the basis of level energies only. However, recent precise ps-lifetime measurements [2,3] using high-statistics coincidence data led to a large set of electromagnetic transition strengths for both nuclei. In combination with large-scale shell model calculations, these data allowed us to pin down the structures of all observed excited states. It was shown that except for the 13^-_2 (6919 keV), 14^-_1 (7970 keV), and 15^-_1 (8133 keV) states in ^{94}Ru, which are proton intruder states, all other levels up to 19^+ (9.9 MeV), 20^- (11.0 MeV) and $39/2^+$ (8.9 MeV), $39/2^-$ (9.3 MeV), respectively, contain a neutron core-excitation. At even higher excitation energies, many high-energy γ-transitions (2-4 MeV) are observed. It is assumed that they depopulate states containing either a second neutron or a $g_{9/2}$ proton being excited across the shell gap. However, for these states neither shell model calculations nor experimental decay strengths are available at the moment.

With the present measurement of magnetic moments in ^{94}Ru and ^{95}Rh we intended to enlarge the experimental basis for the comparison with shell model calculations and to obtain an independent proof of the structural assignments described above. The negative g-factor of a $d_{5/2}$ neutron is expected to lead to a significant reduction of the g-factor for neutron core-excited states as compared to pure proton levels.

Correspondence to: Andrea Jungclaus

2 Experimental details

Our lifetime studies of ^{94}Ru [2] and ^{95}Rh [3] revealed lifetimes in the range between 10 ps and 3 ns for the 12^+ and 11^- yrast states in ^{94}Ru and the $25/2^-$, $29/2^+$, and $35/2^+$ levels in ^{95}Rh. With these lifetimes, the states are accessible to magnetic moment measurements via the IMPAD technique where the time-integral nuclear precessions are observed following the recoil implantation of the excited nuclei into a ferromagnetic host. The precession angles are deduced from the time-integral rotations of the anisotropic angular distributions of γ-rays depopulating the states of interest about the magnetic field direction. The reaction

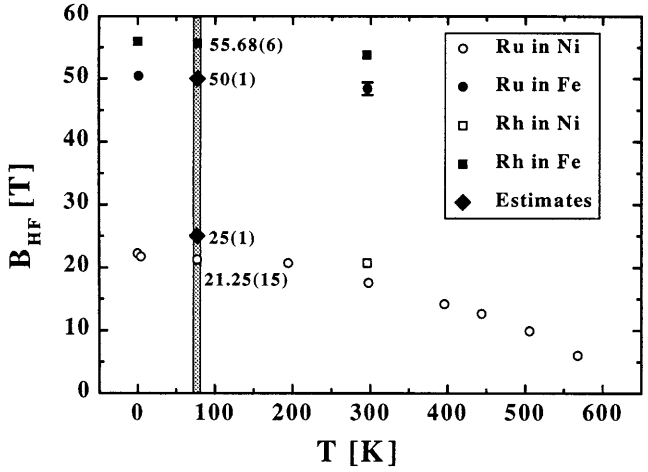

Fig. 1. Hyperfine fields of Tc, Ru, and Rh after recoil-implantation into Fe and Ni hosts [4–6]

Table 1. Static hyperfine fields of Ru and Rh nuclei implanted into Ni and Fe hosts

Nucleus	Z	Fe host		Ni host	
		B_{HF} [T]	$\Delta\Phi/(g\,\tau)$ [mrad/ps]	B_{HF} [T]	$\Delta\Phi/(g\,\tau)$ [mrad/ps]
Ru	44	50(1)	2.39(5)	21.25(15)^a	1.02(1)
Rh	45	55.68(6)^b	2.67(1)	25(1)	1.20(5)

a: from [4], b: from [5]

^{58}Ni + ^{40}Ca was used to populate ^{94}Ru and ^{95}Rh via the reaction channels 4p and 3p with relative experimental cross-sections of 48% and 19%. The 145 MeV 2-particle nA pulsed ^{40}Ca beam was provided by the Heidelberg MP-tandem accelerator. In the first part of the experiment, a 2.3 mg/cm^2 thick ^{58}Ni layer (enrichment 99.8%) backed with a 6.8 mg/cm^2 natural Fe foil was used. Both foils were annealed at 650°C before being glued together with the help of a very thin (100nm) In layer. The thicknesses were chosen such that the recoiling nuclei came to rest in the Fe backing. In the second part, a 9.2 mg/cm^2 ^{58}Ni foil (enrichment 99.8%) was used. Here, Ni served both as target material and ferromagnetic host. Both targets were polarized in a vertical field of 0.15 T provided by an electromagnet. Both the target and the coils of the electromagnet were cooled by liquid nitrogen. The information available on the relevant static hyperfine fields of Ru and Rh in Fe and Ni hosts is summarized in Fig. 1 and Table 1. The hyperfine field experienced by Ru ions in Ni was measured as a function of temperature by Shirley et al. [4]. For 77 K, their measured value is B_{HF}(Ru in Ni)=21.25(15) T. The corresponding value for Rh in Fe is B_{HF}(Rh in Fe)=55.68(6) T at 77 K [5]. For the two remaining ion-host combinations, the hyperfine fields at 77 K have to be extrapolated from the values measured at 4 K and/or room temperature [6]. The uncertainty for this extrapolation is smaller for the Fe host due to the higher Curie temperature of Fe (T_C(Fe)=1043 K) as compared to Ni (T_C(Ni)=627 K). The values we used in our analysis are given in Table 1, together with the expected precession angles $\Delta\Phi/(g\,\tau)$, with g denoting the g-factor and τ the mean lifetime of the nuclear state under consideration, indicating the sensitivity of the different combinations.

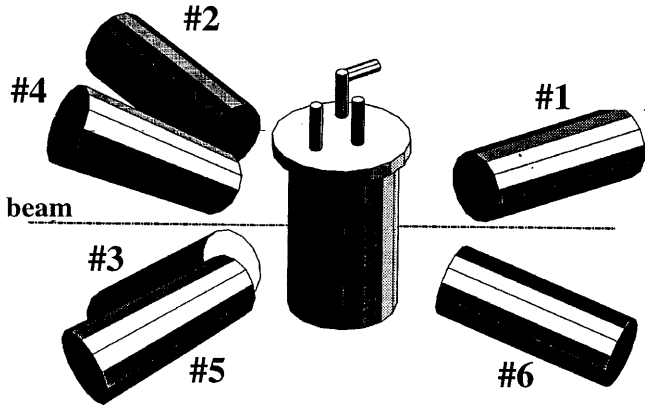

Fig. 2. Six detector setup used in the present IMPAD experiment ($\Theta_{1,6} = \pm 56°$, $\Theta_{2-5} = \pm 124°$)

For detecting the γ-rays, six Ge detectors were positioned around the target as sketched in Fig. 2. Detectors #2-5 (25% efficiency) were placed at angles of Θ_{2-5}=±124° relative to the beam direction with an angle of inclination of about 15° with respect to the horizontal plane (containing the beam axis and being perpendicular to the magnetic field direction). The detectors #1 (70% efficiency) and #6 (54% efficiency) were placed in forward direction at $\Theta_{1,6}$=±56° in the horizontal plane. Throughout the experiment, these two detectors were rotated by $\Delta\Theta$=±4° from these mean positions every hour to allow for a simultaneous measurement of the anisotropy of the γ-ray angular distributions. Singles spectra from the six detectors were accumulated according to their positions (for detectors #1 and #6) and the direction of the polarizing field reversed every two minutes. As an example, the singles spectrum measured in detector #6 for the field direction ↑ is shown in Fig. 3. The strongest lines are labeled

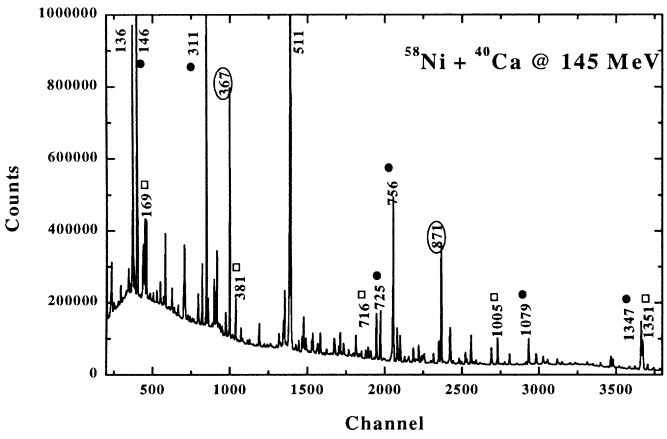

Fig. 3. Singles spectrum measured in detector #6 for field direction ↑. The strongest lines are labeled by their energy and according to the nucleus they belong to. Filled dots: ^{94}Ru, open squares: ^{95}Rh. The 367 and 871 keV γ-rays belong to ^{94}Tc and ^{94}Mo populated after β-decay of ^{94}Ru

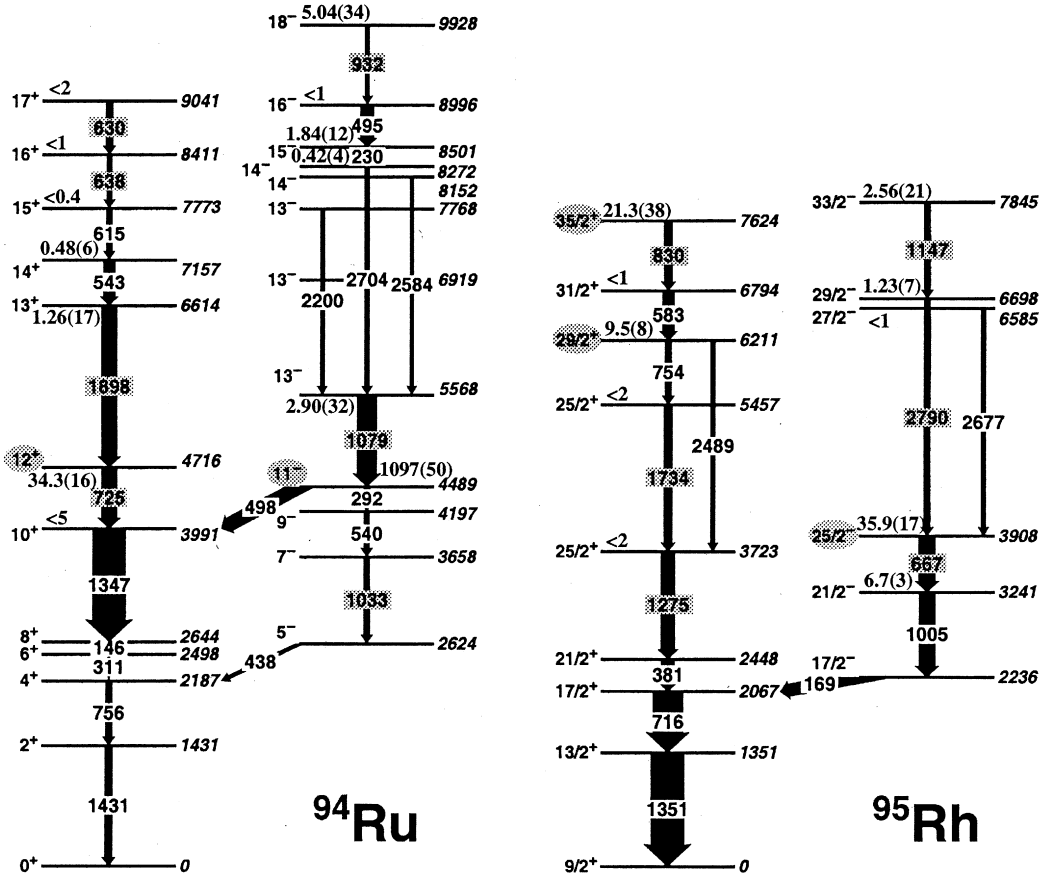

Fig. 4. Partial level schemes of ^{94}Ru and ^{95}Rh (both from [1]) relevant for the present work. Lifetimes in ps are given above the levels (from [2,3])

by the nucleus they belong to in order to indicate the relative strengths of the various reaction channels. This figure also illustrates the general problem of singles measurements, namely the very high line density, which complicates the extraction of the precession angles of individual γ-rays.

To facilitate the following discussion, the relevant parts of the level schemes of ^{94}Ru and ^{95}Rh are given in Fig.4.

3 Data analysis and results

In a first step, the logarithmic slopes of the unpertubed angular distributions of the γ-rays of interest were determined. For each of the two positions $\Theta = \Theta_{1,6} \pm 4°$ of detectors #1 and #6, the original spectra for the two field directions were summed up and from these sum spectra, counting rate double ratios of the form

$$R = \frac{N_1(\Theta_1 + 4°) \cdot N_6(\Theta_6 - 4°)}{N_1(\Theta_1 - 4°) \cdot N_6(\Theta_6 + 4°)} \qquad (1)$$

were calculated, where N_i is the yield of the γ-ray of interest observed in detector #i. The logarithmic slope is obtained from R via the relation

$$S(56°) = \frac{1}{W(56°)} \left. \frac{dW(\Theta)}{d\Theta} \right|_{56°} = \frac{\sqrt{R} - 1}{\sqrt{R} + 1} \cdot \frac{1}{\Delta\Theta} \qquad (2)$$

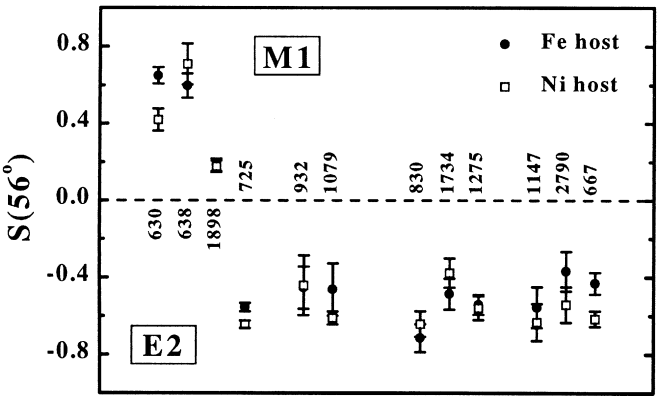

Fig. 5. Experimental logarithmic slopes S(56°) of transitions in ^{94}Ru and ^{95}Rh. The data points are labeled by the γ-ray energy in keV

with $\Delta\Theta = 4°$. This analysis is, of course, only valid for small perturbations (small $\omega\tau$), when the attenuation of the angular distribution can be neglected.

The values $S(56°)$ relevant for the present analysis are plotted in Fig. 5. It should be mentioned that for a typical E2 transition with the angular distribution coefficients a_2=+0.30 and a_4=-0.04, the calculated logarithmic slope for the observation **in** the horizontal plane is

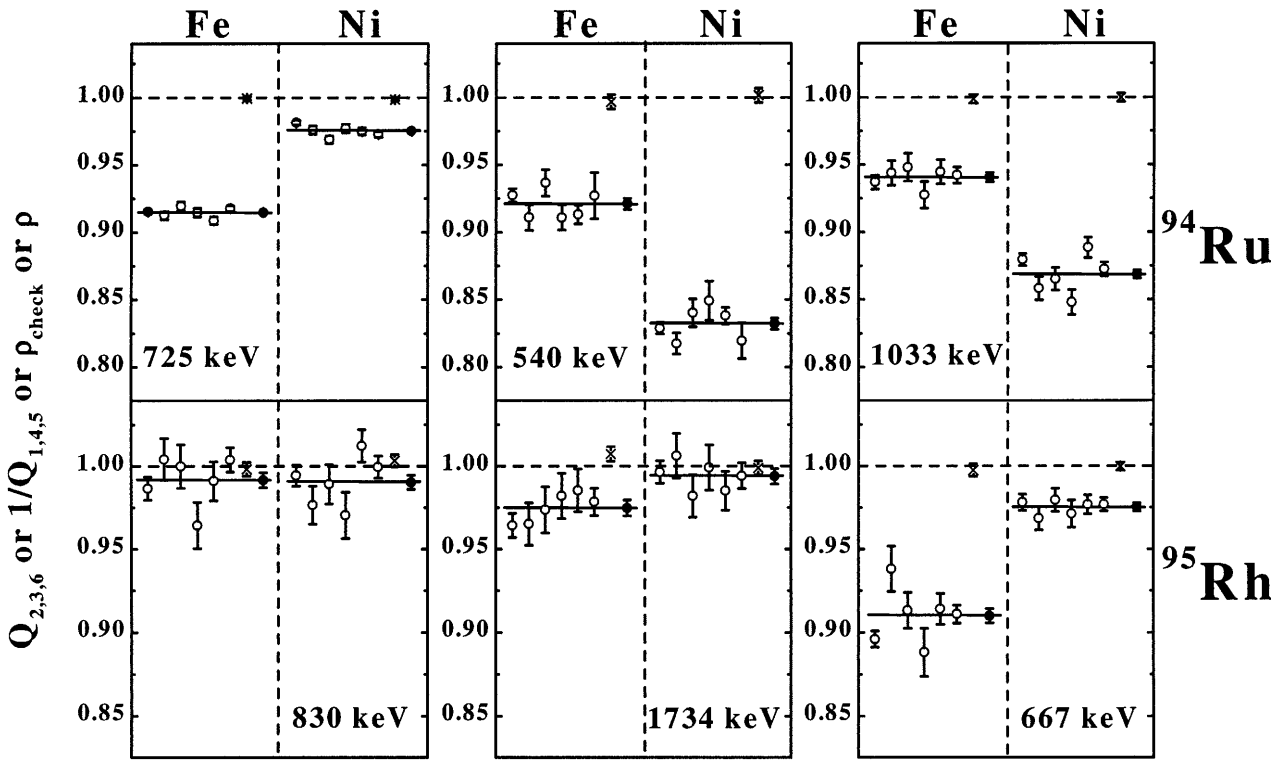

Fig. 6. $Q_{2,3,6}$, $1/Q_{1,4,5}$ (open circles), ρ (filled circles), and ρ_{check} (crosses) values obtained for some transitions in ^{94}Ru and ^{95}Rh for both the Fe and the Ni hosts

S(56°)=-0.45. The corresponding value for observation at an angle of inclination of 15° deviates by only about 4%. The experimental slopes determined from the intensities observed in detectors #1 and #6 can therefore be used for the determination of the precession angles from the spectra taken in all six detectors without introducing any considerable additional uncertainty. As a consistency check, we determined the experimental slopes for γ-rays originating from beam-induced radioactivity in the target and, indeed, their angular distributions were found to be isotropic.

For the determination of precession angles, the counting rate ratios

$$Q_i = \frac{N_i^{\uparrow}}{N_i^{\downarrow}} \tag{3}$$

were calculated from the intensities observed for the two field directions $\uparrow$ and $\downarrow$ in each of the six detectors. These values still depend on the measuring times for the two directions. The ratios Q_2, Q_3, and Q_6 as well as the reciprocal values $1/Q_1$, $1/Q_4$, and $1/Q_5$ should, however, agree within the errors. They are plotted for the γ-rays of interest in Fig. 6 for the two different backings used. No systematic differences are observed, supporting in addition the statement made above concerning the slopes relevant for the out-of-plane detectors.

From the quantity

$$\rho = \left(\frac{Q_2 \cdot Q_3 \cdot Q_6)}{Q_1 \cdot Q_4 \cdot Q_5}\right)^{1/6}, \tag{4}$$

which is independent of detector efficiencies and beam current fluctuations, the precession effect ϵ of the time-integral γ-ray distribution can be derived:

$$\epsilon = \frac{\rho - 1}{\rho + 1}. \tag{5}$$

To check for possible systematic uncertainties due to asymmetries in the detector setup or misalignments of the beam spot on the target, the quantity

$$\rho^{check} = \left(\frac{Q_1 \cdot Q_6}{\sqrt{Q_2 \cdot Q_3 \cdot Q_4 \cdot Q_5}}\right)^{1/4}, \tag{6}$$

which per definition has to agree with unity, was also calculated. Both the values ρ and ρ^{check} for the relevant γ-transitions are shown in Fig. 6.

Finally, the time-integral rotation of a particular angular distribution is given by

$$\Delta\Phi = \frac{\epsilon}{S(56°)}. \tag{7}$$

The experimental results obtained for the two different ferromagnetic hosts are summarized in Table 2.

As mentioned above, this method to extract precession angles is only valid for small perturbations $\omega\tau \ll 1$. However, in the case of the long-lived 11^- state in ^{94}Ru (τ=1097(50) ps [2]), very large precession angles are expected. Assuming a g-factor of g(11^-)=+1 for this state and considering the field strengths for Ru ions implanted into Fe and Ni hosts from Table 1, precession angles of

Table 2. γ-ray energies, observed effects ϵ, experimental logarithmic slopes S(56°) and precession angles $\Delta\Phi$ in ^{94}Ru and ^{95}Rh after recoil-implantation into Fe and Ni hosts

		Fe host				Ni host			
$I_i^\pi \rightarrow I_f^\pi$	E_γ [keV]	ρ	ϵ [10^{-3}]	S(56°)	$\Delta\Phi$ [mrad]	ρ	ϵ [10^{-3}]	S(56°)	$\Delta\Phi$ [mrad]
^{94}Ru									
$17^+ \rightarrow 16^+$	630	0.9835(23)	-8.3(12)	0.650(43)	-12.8(20)	0.9908(43)	-4.6(22)	0.420(58)	-11.0(54)
$16^+ \rightarrow 15^+$	638	0.9797(42)	-10.3(21)	0.597(63)	-17.2(40)	0.9999(89)	-0.1(45)	0.71(11)	-0.1(63)
$13^+ \rightarrow 12^+$	1898	0.9961(19)	-1.95(95)	0.184(32)	-10.6(55)	0.9952(19)	-2.41(95)	0.176(30)	-13.7(59)
$12^+ \rightarrow 10^+$	725	0.9148(11)	-44.50(60)	-0.555(21)	80.2(33)	0.9751(11)	-12.61(56)	-0.644(19)	19.6(11)
				-0.61[a]	74(1)[c]			-0.61[a]	20(1)[c]
				-0.45[b]	104(2)[c]			-0.45[b]	28(1)[c]
$18^- \rightarrow 16^-$	932	1.0072(65)	3.6(32)	-0.45(11)	-7.9(74)	1.0349(130)	17.2(63)	-0.44(16)	-39(20)
$13^- \rightarrow 11^-$	1079	1.0183(20)	9.07(98)	-0.46(14)	-19.6(61)	1.0117(29)	5.8(14)	-0.610(34)	-9.5(24)
$7^- \rightarrow 5^-$	1033	0.9404(34)				0.8686(30)			
				-0.61[a]	$3982(^{258}_{228})$[c]			-0.61[a]	$1630(^{48}_{46})$[c]
				-0.45[b]	$3040(^{200}_{181})$[c]			-0.45[b]	$1168(^{40}_{39})$[c]
^{95}Rh									
$35/2^+ \rightarrow 31/2^+$	830	0.9916(46)	-4.2(23)	-0.715(73)	5.9(33)	0.9903(43)	-4.9(22)	-0.642(66)	7.6(35)
$25/2^+ \rightarrow 25/2^+$	1734	0.9748(48)	-12.8(25)	-0.486(81)	26.2(67)	0.9939(47)	-3.1(24)	-0.378(75)	8.1(65)
$25/2^+ \rightarrow 21/2^+$	1275	0.9823(30)	-8.9(15)	-0.541(51)	16.5(32)	1.0037(46)	1.9(23)	-0.559(62)	-3.3(41)
$33/2^- \rightarrow 29/2^-$	1147	1.0163(68)	8.1(34)	-0.56(11)	-14.5(66)	1.0200(61)	9.9(30)	-0.633(96)	-15.7(53)
$29/2^- \rightarrow 25/2^-$	2790	1.0051(67)	2.5(33)	-0.37(10)	-6.9(92)	1.0037(62)	1.9(31)	-0.542(92)	-3.4(57)
$25/2^- \rightarrow 21/2^-$	667	0.9099(42)	-47.2(23)	-0.431(57)	110(15)	0.9752(26)	-12.6(13)	-0.615(41)	20.4(26)
				-0.61[a]	79(4)[c]			-0.61[a]	20(2)[c]
				-0.45[b]	111(7)[c]			-0.45[b]	28(3)[c]
$21/2^- \rightarrow 17/2^-$	1005	0.9466(17)	-27.43(90)	-0.435(31)	63.0(49)	0.9771(17)	-11.58(87)	-0.414(29)	28.0(29)

a: assuming $a_2 = 0.40$, $a_4 = -0.08$
b: assuming $a_2 = 0.30$, $a_4 = -0.04$
c: $\Delta\Phi = \omega\tau$ deduced by using (11)

$\Delta\Phi_{Ni} = (\omega\tau)_{Ni} = 1.1$ rad and $\Delta\Phi_{Fe} = (\omega\tau)_{Fe} = 2.6$ rad are expected for the γ-rays from the $11^- \rightarrow 9^- \rightarrow 7^- \rightarrow 5^-$ sequence. This means that during the lifetime of the 11^- state, the nuclear magnetic moment rotates by 63° resp. 149° around the magnetic field direction ! In such a case, the attenuation of the angular distribution cannot be neglected any more and the full integral perturbed angular distribution

$$\overline{W^{\uparrow\downarrow}(\Theta)} = \frac{1}{\tau}\int_0^\infty W^{\uparrow\downarrow}(\Theta,t)\, e^{-t/\tau}\, dt = \sum_{k=0,2,4} b_k \frac{cos[k\Theta \pm atan(k\omega\tau)]}{\sqrt{1+k^2(\omega\tau)^2}} \qquad (8)$$

has to be considered. For $W^{\uparrow\downarrow}(\Theta,t)$, the expansion

$$W^{\uparrow\downarrow}(\Theta,t) = \sum_{k=0,2,4} b_k\, cos(k\Theta \pm k\omega t) \qquad (9)$$

was chosen, which is equivalent to the usual expansion in Legendre polynomina P_k

$$W^{\uparrow\downarrow}(\Theta,t) = \sum_{k=0,2,4} a_k\, P_k[cos(\Theta \pm \omega t)] \qquad (10)$$

with the relations $b_0 = 1 + \frac{1}{4}\,a_2 + \frac{9}{64}\,a_4$, $b_2 = \frac{3}{4}\,a_2 + \frac{5}{16}\,a_4$, and $b_4 = \frac{35}{64}\,a_4$. In Fig. 7a), the unperturbed angular distribution $W(\Theta) = 1 + a_2\,P_2(cos\Theta) + a_4\,P_4(cos\Theta)$ with $a_2 = 0.40$ and $a_4 = -0.08$ is compared to the both rotated and attenuated distributions $\overline{W^{\uparrow\downarrow}(\Theta)}$ for two different values of $\omega\tau$. The resulting ratios $\overline{W^{\uparrow}(\Theta)}/\overline{W^{\downarrow}(\Theta)}$ are plotted in Fig. 7b). It is evident that for $\Theta = 56°$ this ratio is very sensitive to the value of $\omega\tau$. With increasing $\omega\tau$, the ratio decreases, but it increases again at a certain value of $\omega\tau$ reaching unity for the limit of infinite $\omega\tau$, where the angular distribution is completely attenuated.

To determine the precession angle of a γ-ray from the experimental quantity ρ (4), the ratio

$$\rho(\omega\tau) = \frac{\overline{W^{\uparrow}(56°,\omega\tau)}}{\overline{W^{\downarrow}(56°,\omega\tau)}} \qquad (11)$$

was calculated as function of the precession angle $\omega\tau$. Concerning the coefficients a_2 and a_4 of the unperturbed angular distribution, assumptions had to be made in the present case. We have chosen two different sets of parameters, namely $a_2 = 0.40$, $a_4 = -0.08$ and $a_2 = 0.30$, $a_4 = -0.04$ ($a_0 = 1$ in both cases). The corresponding values for the logarithmic slopes are S(56°) = -0.61 and S(56°) = -0.45, respectively. These two sets cover the range for typical E2 transitions (compare Fig. 5), leading to reasonable limits for the precession angles. Fig. 8 shows the resulting $\rho(\omega\tau)$ curves. The experimental values for the 1033 keV, $7^- \rightarrow 5^-$ transition below the long-lived 11^- state in ^{94}Ru in both ferromagnetic hosts are marked

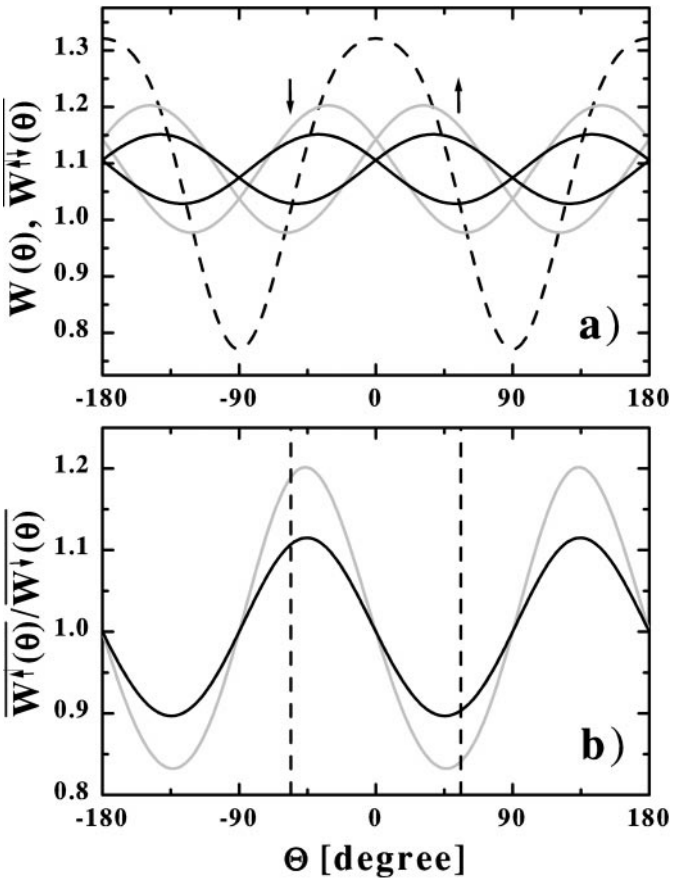

Fig. 7. a) Unperturbed angular distribution $W(\Theta) = 1 + 0.40\,P_2(cos\Theta) - 0.08\,P_4(cos\Theta)$ (dashed line) and perturbed distributions $\overline{W^{\uparrow\downarrow}(\Theta)}$ for $\omega\tau = 1$ rad (grey lines) and $\omega\tau = 2$ rad (black lines). b) Ratios $\overline{W^{\uparrow}(\Theta)}/\overline{W^{\downarrow}(\Theta)}$ for $\omega\tau = 1$ rad (grey line) and $\omega\tau = 2$ rad (black line)

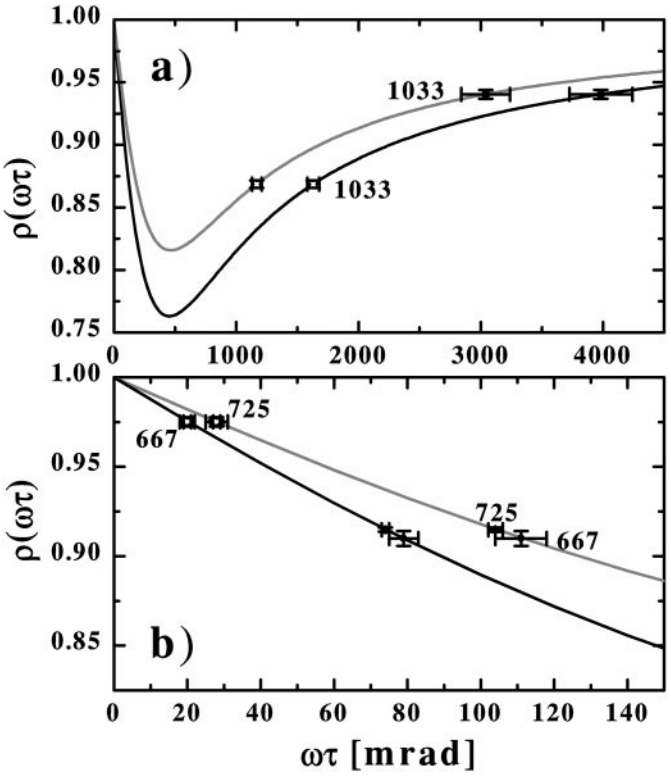

Fig. 8. Calculated functions $\rho(\omega\tau)$ for the two different sets of angular distribution coefficients (black line: a_2=0.40, a_4=-0.08; grey line: a_2=0.30, a_4=-0.04). The experimental ρ values are marked by symbols with error bars (filled symbols: Fe host, open symbols: Ni host)

with error bars in Fig. 8a). For each experimental value ρ, two different precession angles $\omega\tau$ can be read from the $\rho(\omega\tau)$ curves. However, the hyperfine field is much larger in the Fe than in the Ni host, leading to larger precession angles for the Fe host. Since $\rho_{Fe} > \rho_{Ni}$, only the increasing parts of the curves have to be considered. For comparison between the two different methods for determining the precession angles, the values for the 725 keV, $12^+ \rightarrow 10^+$ transition in ^{94}Ru and the $25/2^- \rightarrow 21/2^-$ γ-ray in ^{95}Rh are included in Fig. 8b). In these cases, $\rho_{Ni} > \rho_{Fe}$ in contrast to the situation for the 1033 keV transition (compare Fig. 8a). Here, the down-sloping regions of the $\rho(\omega\tau)$ curves are the relevant ones. As can be seen in Table 2, the agreement is very good in both cases for the a_2, a_4 combination with a value of S(56°) close to the experimental one.

To determine the magnetic moment of a particular state, the net rotation $\Delta\Phi_{net}$ of the nuclear spin during the lifetime of this state has to be deduced. $\Delta\Phi_{net}$ is the difference between the rotation $\Delta\Phi_{out}$ of the depopulating and the weighted mean rotation $\Delta\Phi_{in}$ of the populating transitions. The g-factor is then given by

$$g = -\frac{\hbar}{\mu_N}\frac{\Delta\Phi_{net}}{B_{HF}\cdot\tau} \qquad (12)$$

where B_{HF} is the static hyperfine field and τ the mean lifetime of the state. Due to the short lifetimes above the 12^+ and 11^- levels in ^{94}Ru and the $35/2^+$ and $25/2^-$ states in ^{95}Rh, the rotation of the γ-rays populating these states is not influenced by the static hyperfine field but originates from the experience of transient magnetic fields during the slowing-down process in the ferromagnetic hosts. The average transient field rotations were deduced from the measured precession angles of the 630, 638, 1898, 932, and 1079 keV γ-rays in ^{94}Ru and the 1147 and 2790 keV transitions in ^{95}Rh to be $\Delta\Phi_{Fe}$ = -13(7) mrad and $\Delta\Phi_{Ni}$ = -9(5) mrad.

The g-factor of the 11^- level in ^{94}Ru was obtained from the precession of the subsequent 1033 keV, $7^- \rightarrow 5^-$ γ-ray since the 292 and 540 keV transitions are contaminated in the singles spectra. However, the lifetimes of the 9^- and 7^- states are very short as compared to $\tau(11^-) = 1097(50)$ ps leading only to small contributions to the precession. In the case of the $29/2^+$ state in ^{95}Rh, $\Delta\Phi_{in}$ was taken from the 830 keV, $35/2^+ \rightarrow 31/2^+$ and $\Delta\Phi_{out}$ from the 1734 keV, $25/2^+_2 \rightarrow 25/2^+_1$ transitions. Again, this seems to be legitimate in view of the short lifetimes of the $31/2^+$ and $25/2^+_2$ states and the fact that hardly any sidefeeding into the $31/2^+$ and $29/2^+$ levels is observed. In any case,

Table 3. g-factors in ^{94}Ru and ^{95}Rh deduced from the precession angles $\Delta\Phi$ listed in Table 2 and the hyperfine field strengths from Table 1. In the last two columns, the g-factors from the shell model calculations SM2 and SM3 are given (see text for details)

				Fe host		Ni host					
I^π	τ (ps)	E_γ [keV]		$\Delta\Phi$ [mrad]	g	$\Delta\Phi$ [mrad]	g	g_{ave}	g^a_{est}	g^b_{SM2}	g^b_{SM3}
^{94}Ru											
12^+	34.3(16)	TF	in	-13(7)		-9(5)					
		725	out	80.2(33)		19.6(11)					
			net	93.2(77)	1.13(11)	28.9(51)	0.83(15)	1.03(14)	1.38	1.20(1.21)	1.31(1.37)
11^-	1097(50)	TF	in	-13(7)		-9(5)					
a_2=0.30, a_4=-0.04		1033	out	3040(200)		1168(40)					
			net	3053(200)	1.16(10)	1177(40)	1.05(6)				
a_2=0.40, a_4=-0.08		1033	out	3982(258)		1630(48)					
			net	3995(258)	1.52(12)	1639(48)	1.46(8)	1.28(15)	1.30	1.15(1.15)	1.20(1.23)
^{95}Rh											
$35/2^+$	21.3(38)	TF	in	-13(7)		-9(5)					
		830	out	5.9(33)		7.6(35)					
			net	18.9(77)	0.33(15)	17.0(61)	0.67(27)	0.41(14)	0.57	0.65(0.71)	0.65(0.69)
$29/2^+$	9.5(8)	830	in	5.9(33)		7.6(35)					
		1734	out	26.2(67)		8.1(65)					
			net	20.3(75)	0.80(30)	0.5(74)	0.04(59)	0.64(31)		0.67(0.73)	0.65(0.70)
$25/2^-$	35.9(17)	TF	in	-13(7)		-9(5)					
		667	out	110(15)		20.4(26)					
			net	123(17)	1.28(19)	29.7(56)	0.69(14)	0.90(28)	1.31	1.14(1.13)	0.98(1.23)

a: Estimates assuming pure configurations (see text for details).
b: Results obtained using quenched single-particle resp. effective (in brackets) g-factors.

the g-factor determination for this state is at the limit of the feasible due to its short lifetime of only 9.5 ps.

The g-factors obtained from the precession angles given in Table 2 are listed in Table 3 and plotted in Fig. 9 for both host materials. For the the states with lifetimes in the range 10-35 ps, the results obtained from the measurement with an iron host seem to be somewhat more reliable because the induced effects are larger as compared to the Ni host and, consequently, the influence of the transient field precession is smaller.

4 Discussion

To interprete the g-factor results given in Table 3 we start with the effective single-particle g-factors for protons and neutrons in the relevant orbits deduced experimentally from pure single-particle states in this mass region [6]. These values are compared to the corresponding Schmidt values in Table 4.

Using the Landé formula, we can employ the values from Table 4 to calculate the g-factors of the 12^+ and 11^- states in ^{94}Ru and the $25/2^-$ level in ^{95}Rh assuming pure completely stretched $g_{9/2}$ proton configurations [12^+: $\pi(g_{9/2})^4_{12}$; 11^-: $\pi(g_{9/2})^3_{21/2}$ $\pi(p_{1/2})$; $25/2^-$: $\pi(g_{9/2})^4_{12}$ $\pi(p_{1/2})$]. The values are $g(12^+) = +1.38$, $g(11^-) = +1.30$, and $g(25/2^-) = +1.31$. The $35/2^+$ state should be dominated by the $\pi(g_{9/2})^3_{21/2} \otimes [\nu(g_{9/2})^{-1}\ \nu(d_{5/2})]_7$ configuration since this is the only one with seniority v=5 giving $35/2^+$. In this case the g-factor would be $g(35/2^+) = +0.57$. The negative g-factor of the $d_{5/2}$ neutron leads to a significant decrease of the magnetic moment compared to $g > +1$ for the pure proton states. This is exactly what is observed experimentally.

In a next step we performed full shell model calculations (labeled SM2 and SM3) in extended configuration spaces as described in detail in [2,3]. In the calculation SM2, the spaces ($p_{1/2}$, $g_{9/2}$) for protons and ($g_{9/2}$, $d_{5/2}$, $s_{1/2}$, $d_{3/2}$, $g_{7/2}$) for neutrons and empirical interactions were used [2,7]. In SM3, we included proton excitations from the completely filled $f_{5/2}$, $p_{3/2}$ orbits while for the neutrons only the $d_{5/2}$ orbit above the shell closure was taken into account [3,8]. For calculating g-factors, two different parameter sets were used. First, the single-particle values were employed but with the spin g-factors quenched by a factor of 0.7. These values were also used in the calculation of M1 strengths in our previous work [2,3]. In addition, the effective experimental values given in Table 4 were used. The g-factor results of both calculations are compared in Table 3 to the experimental values. Since the calculated wavefunctions are not pure, small deviations from the more simple estimates g_{est} given above are obtained, as can be seen in Fig. 9. However, the nice agreement between experiment and calculations can be regarded as further support for the structural assignments deduced from the lifetime data [2,3].

Table 4. Theoretical and experimental effective single-particle g-factors

	proton			neutron		
orbit	$g_{Schmidt}$	g^a_{exp}	state^b	$g_{Schmidt}$	g^a_{exp}	state^b
$d_{5/2}$				-0.77	-0.46(1)	$5/2^+$, ^{89}Sr
$g_{9/2}$	+1.51	+1.38(1)	8^+, N=50	-0.43	-0.24(1)	$9/2^+$, ^{87}Sr
$p_{1/2}$	-0.53	-0.28(1)	$1/2^-$, ^{89}Y	+1.28	+1.26(2)	$1/2^-$, ^{87}Sr
$f_{5/2}$	+0.34	+0.34(2)	$5/2^-$, ^{75,77}As			

a: from [6]
b: single particle state from which g_{exp} was derived

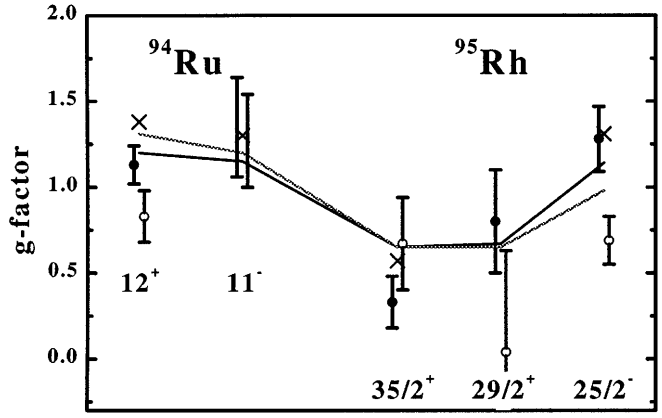

Fig. 9. g-factors in ^{94}Ru and ^{95}Rh. The experimental values are marked by circles (filled: Fe host, open: Ni host), the results from the shell model calculations are plotted as lines (black for SM2, grey for SM3). The g-factors expected for pure configurations (see text) are shown as crosses

5 Conclusions

We used the IMPAD method with both iron and nickel hosts to measure the magnetic moments of the yrast 12^+ and 11^- states in ^{94}Ru and the yrast $29/2^+$, $35/2^+$, and $25/2^-$ levels in ^{95}Rh. In the case of the 11^- state with a lifetime of $\tau = 1097(50)$ ps, very large precession angles of up to 150° were observed so that the data analysis could not be performed in the usual approximation $\omega\tau \ll 1$. The results prove the pure proton character of the 12^+, 11^-, and $25/2^-$ states. The reduced g-factors determined for the $29/2^+$ and $35/2^+$ levels, on the other hand, are clear indications of the neutron core-excited structure of these states.

We are most grateful to the crew of the Heidelberg tandem accelerator for their friendly and efficient cooperation.

References

1. H. A. Roth, S. E. Arnell, D. Foltescu, Ö. Skeppstedt, J. Blomqvist, A. Nilsson, T. Kuroyanagi, S. Mitarai, and J. Nyberg, Phys. Rev. C **50**, (1994) 1330
2. A. Jungclaus, D. Kast, K. P. Lieb, C. Teich, M. Weiszflog, T. Härtlein, C. Ender, F. Köck, D. Schwalm, I. P. Johnstone, J. Reif, R. Schwengner, R. Peusquens, A. Dewald, J. Eberth, H.-G. Thomas, M. Górska, and H. Grawe, Phys. Rev. **C**, 60, (1999) 014309
3. A. Jungclaus, D. Kast, K. P. Lieb, C. Teich, M. Weiszflog, T. Härtlein, C. Ender, F. Köck, D. Schwalm, J. Reif, R. Peusquens, A. Dewald, J. Eberth, H.-G. Thomas, M. Górska, and H. Grawe, Nucl. Phys. **A637**, (1998) 346
4. D. A. Shirley, S. S. Rosenblum, and E. Matthias, Phys. Rev. **170**, (1968) 363
5. G. N. Rao, Hyp. Int. **26**, (1985) 1119
6. P. Raghavan, At. Dat. Nucl. Dat. Tab. **42**, (1989) 189
7. I. P. Johnstone and L. D. Skouras, Phys. Rev. C **55**, (1997) 1227
8. G. Winter, R. Schwengner, J. Reif, H. Prade, L. Funke, R. Wirowski, N. Nicolay, A. Dewald, P. von Brentano, H. Grawe, and R. Schubart, Phys. Rev. C **48** (1993) 1010